

Article

## Detecting chronotaxic systems from single-variable time series with separable amplitude and phase

Gemma Lancaster <sup>1</sup>, Philip T. Clemson <sup>1</sup>, Yevhen F. Suprunenko <sup>1,2</sup>, Tomislav Stankovski <sup>1</sup> and Aneta Stefanovska <sup>1\*</sup>.

<sup>1</sup> Department of Physics, Lancaster University, Lancaster, UK

<sup>2</sup> Institute of Integrative Biology, University of Liverpool, Liverpool, UK

\* Author to whom correspondence should be addressed; aneta@lancaster.ac.uk

Version June 11, 2015 submitted to *Entropy*. Typeset by  $\LaTeX$  using class file *mdpi.cls*

---

1     **Abstract:** The recent introduction of chronotaxic systems provides the means to describe  
2     nonautonomous systems with stable yet time-varying frequencies which are resistant to  
3     continuous external perturbations. This approach facilitates realistic characterization of the  
4     oscillations observed in living systems, including the observation of transitions in dynamics  
5     which were not considered previously. The novelty of this approach necessitated the  
6     development of a new set of methods for the inference of the dynamics and interactions  
7     present in chronotaxic systems. These methods, based on Bayesian inference and detrended  
8     fluctuation analysis, can identify chronotaxicity in phase dynamics extracted from a single  
9     time series. Here, they are applied to numerical examples and real experimental EEG data.  
10    We also review the current methods, including their assumptions and limitations, elaborate  
11    on their implementation, and discuss future perspectives.

12    **Keywords:** Chronotaxic systems; Inverse approach; Nonautonomous dynamical systems;  
13    Bayesian inference; Detrended fluctuation analysis

---

## 14 **1. Introduction**

15 The theory of nonautonomous dynamical systems has increasingly been recognised as necessity in the  
16 treatment of the inherent time-variability of biological systems [1]. Closer inspection of the dynamics  
17 observed in nature suggests that previous approaches to the characterization of temporal fluctuations  
18 in these observations may be insufficient. At first glance, biological fluctuations may appear random,  
19 leading to their description by stochastic models [2]. The complexity observed in biological systems has  
20 also led to attempts to treat them with chaos theory [3], however this does not allow for the apparent  
21 stability of these systems, irrespective of their initial conditions. Such characteristics of biological  
22 oscillators suggests underlying determinism or control of both their amplitudes and frequencies even  
23 with continuous perturbations. This phenomenon of biological systems resisting a natural tendency to  
24 disorder was discussed in terms of free energy minimization [4] and separation of internal and external  
25 states, but this approach is still based on random dynamics. A closely related yet more natural approach  
26 is to consider them as nonautonomous systems, which are explicitly time dependent. Approaches  
27 based on reformulation of nonautonomous systems as higher dimensional autonomous systems introduce  
28 unnecessary complexity whilst failing to accurately describe dynamics arising from nature, due to the  
29 fact that these are open systems, subject to continuous variable external perturbations. Many living  
30 systems may be considered as nonautonomous oscillatory systems, with such time-varying dynamics  
31 observed in individual mitochondria [5], the cardio-respiratory system [6,7], the brain [8] and blood flow  
32 [9].

33 Although stability of the amplitude dynamics of an oscillator can be achieved with autonomous  
34 self-sustained limit cycle oscillators, the frequency of this oscillation could be easily changed by weak  
35 external perturbations [10]. To account for a case where this frequency of oscillation is also robust  
36 to perturbations, yet time dependent, a completely new approach is required. Thus, nonautonomous  
37 systems with stable yet time-varying frequencies were recently addressed, and formulated as chronotaxic  
38 systems [10–12]. Chronotaxic systems possess a time-dependent point attractor provided by an external  
39 drive system. This allows the frequency of oscillations to be prescribed externally through this driver  
40 and response system, giving rise to determinism even when faced with strong perturbations.

41 Once these properties of the underlying system have been recognised, the next problem is how to  
42 infer these dynamics and interactions from direct observations, i.e. via the inverse approach. In a  
43 chronotaxic system, particularly one found in nature, whilst the underlying dynamics are defined by the  
44 external driver, the system will likely still be affected by other influences and noise, and these may mask  
45 the chronotaxic dynamics if the correct analytical approach is not applied. For example, the inherent  
46 time-variability of the frequency of the dynamics arising from a chronotaxic system means that it cannot  
47 be accurately characterized by any method based on averaging. This novel class of systems requires new  
48 inverse approach methods, with the focus on the extraction and identification of the dynamics of the drive  
49 system, and its influence on the response system. Here, we review the current state of inverse approach  
50 methods for the identification of chronotaxicity, from a *single time series* of the response system in  
51 which the phase and amplitude dynamics are separable. We then apply these methods to numerically  
52 simulated and real experimental data. Section 2 presents the mathematical formulation of chronotaxic  
53 systems, Section 3 describes current inverse approach methods and their application to the detection

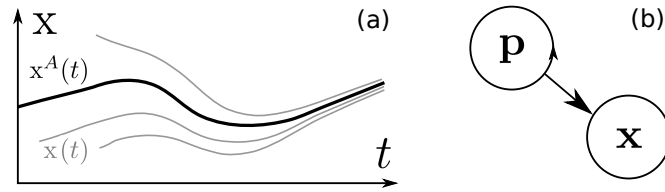


**Figure 1.** (a) Moving point attractor, (b) simplest case of a chronotaxic system

of chronotaxicity. In Section 4, numerical examples are presented to demonstrate the methods, and their assumptions and limitations are discussed. The inverse approach methods are also applied to real experimental data. Finally, Section 5 discusses future directions of the work.

## 2. Chronotaxic systems

The crucial concept in the theory of chronotaxic systems is the ability to resist continuous external perturbations. In autonomous systems, such an ability is provided by a stationary steady state, allowing the system to always return to the vicinity of this steady state when continuously externally perturbed. However, only in nonautonomous (thermodynamically open) systems can the position of this steady state change in time, i.e. be outside of equilibrium. In such a case, not only the stationary state of a system, but also its time-dependent dynamics will be able to resist continuous external perturbations. These oscillatory nonautonomous dynamical systems with time-dependent steady states were introduced in Ref. [10] and named chronotaxic systems, emphasizing that their dynamics is ordered in time (*chronos* – time, *taxis* – order).

Mathematically, nonautonomous dynamical systems and, consequently, chronotaxic systems, are defined by the following system of equations,

$$\dot{\mathbf{p}} = \mathbf{f}(\mathbf{p}); \quad \dot{\mathbf{x}} = \mathbf{g}(\mathbf{x}, \mathbf{p}). \quad (1)$$

where  $\mathbf{p} \in R^n$ ,  $\mathbf{x} \in R^m$ ,  $\mathbf{f} : R^n \rightarrow R^n$ ,  $\mathbf{g} : R^m \times R^n \rightarrow R^m$ , where  $n$  and  $m$  can be any positive integers. Importantly, the solution  $\mathbf{x}(t, t_0, \mathbf{x}_0)$  of Eqs. (1) depends on the actual time  $t$  as well as on the initial conditions  $(t_0, \mathbf{x}_0)$ , whereas the solution  $\mathbf{p}(t - t_0, \mathbf{p}_0)$  depends only on initial condition  $p_0$  and on the time of evolution  $t - t_0$ . The subsystem  $\mathbf{x}$  is nonautonomous in a sense that it can be described by an equation which depends on time explicitly, e.g.  $\dot{\mathbf{x}} = \mathbf{g}(\mathbf{x}, \mathbf{p}(t))$ . A chronotaxic system is described by  $\mathbf{x}$  which is assumed to be observable, and  $\mathbf{p}$  which may be inaccessible for observation, as often occurs when studying real systems. Rather than assuming or approximating the dynamics of  $\mathbf{p}$ , we focus on the dynamics of  $\mathbf{x}$  and use only the following simple assumption: system  $\mathbf{p}$  is assumed to be such that it creates a time-dependent steady state in the dynamics of  $\mathbf{x}$ , which is schematically shown in Fig. 1(a).

Therefore, the whole external environment with respect to  $\mathbf{x}$  is divided into two parts. The first part is given by  $\mathbf{p}$  which is only that part which makes the system  $\mathbf{x}$  chronotaxic (defined below), i.e. an unperturbed chronotaxic system. The second part contains the rest of the environment and is therefore considered as external perturbations.

Firstly, we provide a mathematical formulation of unperturbed chronotaxic systems. The defining component of an unperturbed chronotaxic system is a time-dependent steady state, also called a point attractor, and denoted  $\mathbf{x}^A(t)$ . Usually, a steady state is defined using a so-called forward limit, i.e. when forward time approaches infinity. Assuming that the whole space  $R^m$  of  $\mathbf{x}$  is a basin of attraction, i.e.

that for any initial condition  $\mathbf{x}_0$  at time  $t_0$  the solution of the system asymptotically approaches the time-dependent steady state  $\mathbf{x}^A$ , a condition of forward attraction for  $\mathbf{x}^A$  is the following,

$$\lim_{t \rightarrow +\infty} |\mathbf{x}(t, t_0, \mathbf{x}_0) - \mathbf{x}^A(t)| = 0. \quad (2)$$

This condition can only be satisfied when the chronotaxic system is not perturbed. However, taking into account the time-dependence of  $\mathbf{x}^A(t)$ , this condition is not satisfactory in terms of defining the time-dependent point attractor. Any solution  $\tilde{\mathbf{x}}(t, t_0, \mathbf{x}_0)$  which satisfies (2) with given  $\mathbf{x}^A(t)$  can also be considered as a time-dependent point attractor. Moreover, when dealing with living systems, it is crucially important to describe stability at the current time  $t$  and not in the infinite future. This problem is resolved by employing a condition of pullback attraction, which should also be satisfied by  $\mathbf{x}^A(t)$  in a chronotaxic system,

$$\lim_{t_0 \rightarrow -\infty} |\mathbf{x}(t, t_0, \mathbf{x}_0) - \mathbf{x}^A(t)| = 0. \quad (3)$$

One can see, that this condition defines a time-dependent point attractor at current time  $t$ . Considering the condition (3) at all times  $t > -\infty$ , it follows that the time-dependent point attractor should also satisfy the invariance condition, i.e. the condition that  $\mathbf{x}^A$  is a solution of the system (1),

$$\mathbf{x}(t, t_0, \mathbf{x}^A(t_0)) = \mathbf{x}^A(t). \quad (4)$$

80 Equations (2) and (3) determine asymptotic convergence in the infinite future or starting from the  
 81 infinite past. Asymptotic convergence allows the dynamics of  $\mathbf{x}(t, t_0, \mathbf{x}_0)$  to deviate from  $\mathbf{x}^A$  during a  
 82 certain finite time interval. Therefore, during this time-interval the ability to resist continuous external  
 83 perturbations will be absent. Therefore, in order to characterize the ability of living systems to sustain  
 84 their time-dependent dynamics at finite time intervals, chronotaxic system should satisfy the condition of  
 85 contraction, or equivalently the attraction at all times. This means that in the phase space  $R^m$ ,  $\mathbf{x} \in R^m$ ,  
 86 there should be a contraction region  $C(t)$  such that for any two trajectories  $\mathbf{x}_1, \mathbf{x}_2$  of a system inside the  
 87 contraction region  $\mathbf{x}_i(t, t_0, \mathbf{x}_{0i}) \in C(t)$ ,  $i = 1, 2$ , the distance between them can only decrease,

$$\frac{d}{dt} |\mathbf{x}_1(t, t_0, \mathbf{x}_{01}) - \mathbf{x}_2(t, t_0, \mathbf{x}_{02})| < 0. \quad (5)$$

88 However, in general the contraction region  $C(t)$  can be finite, and different trajectories can eventually  
 89 leave this region. Therefore, in a chronotaxic system the contraction region should contain a finite area  
 90  $A'$ ,  $A' \subset C$ , such that solutions of the system starting in  $A'$  never leave it,  $\forall t_0 < t, \forall \mathbf{x}_0 \in A'(t_0)$ ,  
 91  $\mathbf{x}(t, t_0, \mathbf{x}_0) \in A'(t)$ . In such a case, fulfillment of these conditions guarantees that the time-dependent  
 92 point attractor  $\mathbf{x}^A$  is located inside the area  $A'$  inside the contraction region  $C$ .

Alternatively, the trajectory  $\mathbf{x}^A(t)$  can be viewed as a linearly attracting uniformly hyperbolic trajectory [13], so that the distance between a neighboring trajectory and  $\mathbf{x}^A(t)$  can only decrease in an unperturbed chronotaxic system. For more details and for relations between chronotaxic and other dynamical systems see Ref. [12]. A simple example of an unperturbed chronotaxic system is given by unidirectionally coupled phase oscillators with unwrapped phase  $\varphi_{\mathbf{x}} \in (-\infty, \infty)$  driven by a phase  $\varphi_{\mathbf{p}} \in (-\infty, \infty)$ :

$$\dot{\varphi}_{\mathbf{x}} = \omega_0(t) - \varepsilon(t) \sin(\varphi_{\mathbf{x}} - \varphi_{\mathbf{p}}(t)), \quad (6)$$

93 where  $\dot{\varphi}_{\mathbf{p}}(t) = \omega(t)$ . The point attractor will exist if the condition of chronotacticity [11] is fulfilled,  
94  $|\varepsilon(t)| > |\omega_0(t) - \omega(t)|$ . As an example, for a particular choice  $\varepsilon(t) = \omega(t) > 0$ , and  $\omega_0(t) = 0$ , the  
95 equation can be integrated, and the limit  $t_0 \rightarrow -\infty$  can be calculated, leading to the explicit expression  
96 for a time-dependent point attractor of an unperturbed chronotactic system,  $\varphi_{\mathbf{x}}^A(t) = \varphi_{\mathbf{p}}(t) - \pi/2 + 2\pi k$ ,  
97 and  $k$  is any integer.

98 It should be noted that the dynamics of  $\mathbf{p}$  can be complex or stochastic, or chaotic, provided that the  
99 above conditions are met. Nevertheless, the dynamics of  $\mathbf{x}$  will be determined by the dynamics of  $\mathbf{p}$ ,  
100 and therefore it will be deterministic, at least in unperturbed chronotactic systems. When considering  
101 perturbed chronotactic systems, for simplicity it is sufficient to consider perturbations only to the  $\mathbf{x}$   
102 component, as any perturbations to  $\mathbf{p}$  can be included in its dynamics assuming that  $\mathbf{x}$  does not  
103 influence  $\mathbf{p}$ . In perturbed chronotactic systems, which model real life systems, the general external  
104 perturbations will create complex dynamics of  $\mathbf{x}$  with a stochastic component. Such dynamics may  
105 look very complex: perturbations can push trajectories away from the contraction region, therefore they  
106 can temporarily deviate before they converge. Despite this, due to the existence of the contraction  
107 region, the system will resist continuous external perturbations. The time-dependent dynamics of a  
108 perturbed chronotactic system will be very close to the dynamics of the unperturbed chronotactic system  
109 provided the perturbations are weak enough. In the case of very strong continuous perturbations, such  
110 perturbations may override the driving system  $\mathbf{p}$ , and become effectively a new driver, causing the initial  
111 point attractor of the chronotactic system to disappear. However, it may be restored once the perturbations  
112 again become sufficiently weak.

113 Thus, when perturbations do not destroy the chronotactic properties of a system, the stable  
114 deterministic component of its dynamics can be identified, as will be shown below. This reduces the  
115 complexity of the system, allowing us to filter out the stochastic component and focus on deterministic  
116 dynamics and interactions between system  $\mathbf{x}$  and its driver  $\mathbf{p}$ , [10,14]. For such complex systems as  
117 living systems, it has the potential to extract properties of the system which were previously neglected.

### 118 3. Inverse approach for chronotactic systems

#### 119 3.1. Inverse approaches to nonautonomous dynamical systems

120 A wide range of observed properties in living systems can be explained by considering them as  
121 nonautonomous. Despite this, difficulties in their analysis as such have led to many unsuccessful attempts  
122 to apply methods more suited to autonomous systems. From a single time series arising from a dynamical  
123 system, inverse approach methods can be used to infer the underlying dynamics of this system, in terms  
124 of phase or amplitude. In deterministic systems, phase space analysis is usually the first point of call,  
125 i.e. reconstruction of the attractor in phase space. This can be achieved with only a single time series  
126 using embedding, in which the dimensions of the reconstructed attractor are composed of time-delayed  
127 versions of the data in the time series [15]. This approach works well for autonomous systems, but does  
128 not consider the possibility of time-dependent attractors [1]. Phase space methods are particularly suited  
129 to the treatment of the dynamics observed in chaotic systems, however, nonautonomous systems appear

130 very complex in phase space. To incorporate time-dependence into these systems, extra dimensions in  
131 phase space are required, introducing unnecessary complexity to the problem.

132 In the case that there is only one oscillation in the time series, the Hilbert transform can be applied  
133 to obtain the complex analytic signal, from which the instantaneous phase can be determined directly. If  
134 the time series contains more than one component of interest, for example different oscillatory modes,  
135 it can be decomposed into its constituent parts using a method such as empirical mode decomposition  
136 (EMD), in which peak/trough detection is used to create upper and lower envelopes. From these, a  
137 trend is defined and subtracted from the signal to produce a series of intrinsic mode functions, each one  
138 representing an oscillatory component of the time series [15]. However, there are some limitations when  
139 applying EMD to nonstationary data.

140 Many signal analysis methods assume stationarity of the frequency distribution of the data, but in  
141 nonautonomous systems this assumption is not valid. Single variable time-series, particularly those  
142 from living systems, must be treated as arising from nonautonomous dynamical systems, due to  
143 time-dependent influences of variables other than the one under study. Approaches based on windowing  
144 have been applied in order to attempt to treat time-variability in data, but these potentially lose crucial  
145 information. For example, in phase space reconstruction, the window may not be of a sufficient size  
146 to capture the whole of the attractor, or its variations in time. Application of the Fourier transform to  
147 nonstationary data will result in a blurred or misleading power spectra, severely limiting its usefulness.  
148 The windowing approach has been applied here with some success, in the form of the Short Time Fourier  
149 transform (STFT), but the use of windowing leads to limitations; the better the time resolution, the  
150 worse the frequency resolution (known as the Gabor limit [16]). In addition, the fixed time-frequency  
151 relationship at all scales in a windowed Fourier transform severely limits its usefulness for the analysis  
152 of low frequency oscillations. This problem can be addressed by using the continuous wavelet transform  
153 (CWT), which provides a logarithmic frequency scale (see Section 3.3). The CWT is based on wavelets  
154 rather than the sines and cosines used in Fourier based methods. The simultaneous observation of the  
155 time and frequency domains is extremely useful in the visualization of dynamical systems and their  
156 time evolution. As a result, development of wavelet-based methods specifically for the treatment of  
157 time-dependent dynamics is now a very active field of research [15], including wavelet phase coherence  
158 [17], the synchrosqueezed transform [18,19] and wavelet bispectrum .

159 In addition to determining the characteristics of the underlying dynamics of single nonautonomous  
160 oscillatory modes, inverse approach methods are also used to decompose their interactions. One  
161 of the most well known characteristics of interacting systems is synchronization between oscillatory  
162 components, i.e. a fixed relationship between their phases or amplitudes. Once the phases of  
163 oscillations have been extracted from a time series, a measure of phase synchronization can be  
164 calculated using synchronization indices or phase coherence [15]. However, these methods do not  
165 account for time-varying synchronization. Dynamical Bayesian inference is able to detect time-varying  
166 synchronization in a system, whilst simultaneously inferring the direction of coupling and time-evolving  
167 coupling functions [20,21]. In the time-frequency domain, wavelet phase coherence can be used to  
168 monitor phase relationships over time and frequency by utilising the phase information obtained from  
169 the continuous wavelet transform [15,17]. In a similar way, couplings between oscillators can be detected

170 and quantified using wavelet bispectrum [22]. The ability of these methods to directly take into account  
 171 the time-varying characteristics of data makes them ideal for application to nonautonomous systems.

### 172 3.2. Detecting chronotaxicity

173 Here we present two distinct inverse approach methods which may be utilised in the detection  
 174 of chronotaxicity: phase fluctuation analysis (PFA) and dynamical Bayesian inference. It should be  
 175 noted that the current methods are only applicable to phase dynamics in the context of the detection of  
 176 chronotaxicity, i.e. we focus on the ability of the time-varying frequency to resist continuous external  
 177 perturbations. The two methods rely on a different inferring basis. Phase fluctuation analysis provides a  
 178 measure of statistical effects observed in a signal, whilst the dynamical Bayesian inference method infers  
 179 a model of differential equations and gives a measure of dynamical mechanisms, i.e. the evaluation  
 180 of chronotaxicity relies on the inferred parameters of the model. PFA is said to infer a functional  
 181 connectivity, while the dynamical Bayesian inference method infers effective connectivity [23]. The  
 182 optimal method to use depends on the characteristics of the data, as detailed below.

It is possible to detect whether a system is chronotaxic or not by observing the distribution of the fluctuations in the system relative to its unperturbed trajectory. This comes from the fact that if the original distribution of the perturbations is known, then the stability of the system relative to the unperturbed trajectory (which by definition follows the time-dependent point attractor in a chronotaxic system) can be determined from how these perturbations grow or decay over time. For example, take the non-chronotaxic phase oscillator [24]

$$\dot{\varphi}_{\mathbf{x}} = \omega_0(t) + \eta(t), \quad (7)$$

where  $\omega_0(t)$  is the time-dependent natural frequency and the observed phase  $\varphi_x$  is perturbed by noise fluctuations  $\eta(t)$ . Integrating we find,

$$\varphi_{\mathbf{x}} = \int \omega_0(t)dt + \int \eta(t)dt. \quad (8)$$

Assuming that  $\omega_0(t) > 0$  and  $\eta(t)$  is an uncorrelated Gaussian process, this means that the dynamics of  $\varphi_{\mathbf{x}}$  will consist of a monotonically increasing phase perturbed by a random walk noise (Brownian motion). However, the situation is different for a chronotaxic phase oscillator, e.g.

$$\begin{aligned} \dot{\varphi}_{\mathbf{p}} &= \omega_0(t), \\ \dot{\varphi}_{\mathbf{x}} &= \varepsilon\omega_0(t) \sin(\varphi_{\mathbf{p}} - \varphi_{\mathbf{x}}) + \eta(t), \end{aligned} \quad (9)$$

183 where  $\varphi_{\mathbf{p}}$  is an external phase and  $|\varepsilon| > 1$ . In this case the stability provided by the point attractor  
 184 causes each noise perturbation to decay over time, preventing  $\eta(t)$  from being integrated over to the  
 185 same extent. The perturbations still do not decay instantly as the system takes time to return to the point  
 186 attractor, meaning that some integration of the noise still takes place. However, the size of the observed  
 187 perturbations over longer timescales is greatly reduced, causing a change in the overall distribution from  
 188 that expected for Brownian motion.

### 189 3.3. Extracting the perturbed and unperturbed phases

190 The first problem of generating a method based on the above principle is how to extract both the  
 191 perturbed and unperturbed phases of the system from an observed time series. This usually requires  
 192 the separation of the amplitude and phase for an oscillation in the time series, which is possible using  
 193 time-frequency domain analysis [15]. The analytic signal generated by the Hilbert transform can also  
 194 be used but this requires corrections for nonlinear oscillations and cannot be used when more than one  
 195 oscillation is present in the time series [14,25,26]. Additionally, the use of the Hilbert transform requires  
 196 the use of protophase-to-phase conversion [26].

A time-frequency representation with an optimal frequency resolution of the time series  $f(t)$  of length  $L$  is provided by the continuous wavelet transform [27],

$$W_T(s, t) = \int_0^L \Psi(s, u - t) f(u) du, \quad (10)$$

where  $\Psi(s, t)$  is the mother wavelet, which is scaled according to the parameter  $s$  to change its frequency distribution and time-shifted according to  $t$ . The Morlet wavelet is a commonly used mother wavelet and is defined as [28],

$$\Psi(s, t) = \frac{1}{\sqrt[4]{\pi}} \left( e^{\frac{2\pi i f_0 t}{s}} - e^{-\frac{2\pi f_0^2}{2}} \right) e^{-\frac{t^2}{2s^2}}, \quad (11)$$

197 where the corresponding frequency is given by  $1/s$  and  $f_0$  is a parameter known as central frequency  
 198 which defines the time / frequency resolution [27].

199 Oscillations can be traced in  $W_T(s, t)$  using either a ridge-extraction method [29,30] or the  
 200 synchrosqueezed wavelet transform (SWT) [18]. These extraction methods can be used to estimate  
 201 the instantaneous frequencies of the oscillatory components in a time series, allowing identification of  
 202 harmonics which can be used to determine the intra-cycle dynamics. The phase  $\varphi_x$  of the observed  
 203 system is then  $\arg(W_T(s, t))$ , where  $s$  and  $t$  denote the positions of the oscillation in the  $s - t$  plane.

204 With the estimated perturbed phase  $\varphi_x^*$  extracted, further work is needed to obtain the unperturbed  
 205 phase  $\varphi_x^{A*}$ . In particular, it is difficult to separate the dynamics corresponding to  $\varphi_x^A$  from the effect of  
 206 the noise perturbations  $\eta(t)$ . This task is simplified by assuming that the dynamics of  $\varphi_x^A$  are confined  
 207 to timescales larger than a single cycle and that the noise is either weak or comparable in magnitude to  
 208 these dynamics.

209 With these assumptions, an estimate of  $\varphi_x^A$  can be found by filtering out high-frequency components  
 210 of  $\varphi_x^*$ . However, such a filter should not smooth over the dynamics of  $\varphi_x^A$ . An optimal way of removing  
 211 these high-frequency noise fluctuations without affecting the unperturbed dynamics is to instead smooth  
 212 over the frequency extracted from the wavelet transform [15]. This provides the estimated angular  
 213 velocity  $\dot{\varphi}_x^A$ , which can in turn be integrated over time to give the estimated phase of the driver  $\varphi_x^{A*}$ .  
 214 For further methodological details on phase extraction see Section 4.2.

### 215 3.4. Dynamical Bayesian inference

216 One approach to the detection of chronotoxicity is the application of dynamical Bayesian inference to  
 217 the extracted perturbed ( $\varphi_x^*$ ) and unperturbed ( $\varphi_x^{A*}$ ) phase estimates in order to model their interactions.

218 In dynamical systems Bayesian inference can simultaneously detect time-varying synchronization,  
 219 directionality of coupling and time-evolving coupling functions [20,21]. The characteristics of these  
 220 coupling functions between  $\varphi_x^*$  and  $\varphi_x^{A*}$  may reveal the dynamic mechanisms of the system in terms of  
 221 chronotaxicity. Bayesian inference is able to track time-dependent system parameters, meaning that it is  
 222 particularly useful for the detection of chronotaxicity in systems which move in and out of a chronotaxic  
 223 state.

224 Following extraction of phases from the continuous wavelet transform, as described in Section 3.3,  
 225 we assume their dynamics is described by [14,20,21]

$$\dot{\varphi}_i = \omega_i + f_i(\varphi_i) + g_j(\varphi_i, \varphi_j) + \xi(t), \quad (12)$$

226 where  $\omega_i$  is the natural frequency of the oscillation,  $f_i(\varphi_i)$  are the self-dynamics of the phase,  $g_i(\varphi_i, \varphi_j)$   
 227 are the cross couplings, and  $\xi(t)$  is a two-dimensional white Gaussian noise  $\langle \xi_i(t)\xi_j(\tau) \rangle = \delta(t - \tau)E_{ij}$ .  
 228 Based on the periodic nature of the system, the basis functions are modeled using the Fourier bases

$$f_i(\varphi_i) = \sum_{k=-\infty}^{\infty} \tilde{a}_{i,2k} \sin(k\varphi_i) + \tilde{a}_{i,2k+1} \cos(k\varphi_i), \quad (13)$$

229 and

$$g_i(\varphi_i, \varphi_j) = \sum_{s=-\infty}^{\infty} \sum_{r=-\infty}^{\infty} \tilde{b}_{i,r,s} e^{2\pi i r \varphi_i} e^{2\pi i s \varphi_j}, \quad (14)$$

230 where  $k, r, s \neq 0$ . In practice, it is reasonable to assume that the dynamics will be well described by a  
 231 finite number of Fourier terms, denoted  $A_{i,k}(\varphi_i, \varphi_j)$ . The corresponding parameters from  $\tilde{a}_i$  and  $\tilde{b}_i$  then  
 232 form the parameter vector  $c_k^{(i)}$ . The inference of these parameters utilises Bayes' theorem,

$$p_{\mathcal{X}}(\mathcal{M}|\mathcal{X}) = \frac{\ell(\mathcal{X}|\mathcal{M})p_{\text{prior}}(\mathcal{M})}{\int \ell(\mathcal{X}|\mathcal{M})p_{\text{prior}}(\mathcal{M})d\mathcal{M}}, \quad (15)$$

233 where  $p_{\mathcal{X}}(\mathcal{M}|\mathcal{X})$  is the posterior probability distribution and  $\ell(\mathcal{X}|\mathcal{M})$  is the likelihood function for the  
 234 values of the model parameters  $\mathcal{M}$  given the data  $\mathcal{X}$ , and  $p_{\text{prior}}(\mathcal{M})$  is a prior distribution. The negative  
 235 log-likelihood function is

$$S = \frac{N}{2} \ln |E| + \frac{h}{2} \sum_{n=0}^{N-1} \left( c_k^{(l)} \frac{\partial A_{l,k}(\varphi_{\cdot,n})}{\partial \varphi_l} + [\dot{\varphi}_{i,n} - c_k^{(i)} A_{i,k}(\varphi_{\cdot,n})](E^{-1})_{i,j} [\dot{\varphi}_{j,n} - c_k^{(j)} A_{j,k}(\varphi_{\cdot,n})] \right), \quad (16)$$

236 with implicit summation over repeated indices  $k, l, i, j$ . The log-likelihood is a function of the Fourier  
 237 coefficients of the phases [20].

238 Assuming a multivariate normal distribution as the prior for parameters  $c_k^{(i)}$  with means  $\bar{c}$  and  
 239 covariances  $\Sigma = \Xi^{-1}$ , the stationary point of S can be calculated recursively from

$$\begin{aligned}
E_{i,j} &= \frac{\hbar}{N} [\dot{\varphi}_{i,n} - c_k^{(i)} A_{i,k}(\varphi_{\cdot,n}^*)] [\dot{\varphi}_{j,n} - c_k^{(j)} A_{j,k}(\varphi_{\cdot,n}^*)], \\
c_k^{(i)} &= (\Xi^{-1})_{kw}^{i,l} r_w^{(l)}, \\
r_w^{(l)} &= (\Xi_{prior})_{kw}^{(i,l)} c_w^{(l)} + \hbar A_{i,k}(\varphi_{\cdot,n}^*) (E^{-1})_{ij} \dot{\varphi}_{j,n} - \frac{\hbar}{2} \frac{\partial A_{l,k}(\varphi_{\cdot,n})}{\partial \varphi^l}, \\
\Xi_{kw}^{i,j} &= \Xi_{prior kw}^{i,j} + \hbar A_{i,k}(\varphi_{\cdot,n}^*) (E^{-1})_{ij} A_{j,w}(\varphi_{\cdot,n}^*).
\end{aligned} \tag{17}$$

240 These are calculated within a moving time window, with the posterior of each window becoming  
241 the prior of the next. The inferred parameters of the basis functions can be used to determine  
242 whether synchronization results. The presence of synchronization provides evidence that the system  
243 is chronotaxic, however it remains unclear from which coupling function the stability arises without  
244 calculating the direction of coupling [31],

$$D = \frac{\epsilon_{12} - \epsilon_{21}}{\epsilon_{12} + \epsilon_{21}}, \tag{18}$$

245 where

$$\begin{aligned}
\epsilon_{12} &= \sqrt{c_2^2 + c_4^2 + \dots}, \\
\epsilon_{21} &= \sqrt{c_1^2 + c_3^2 + \dots},
\end{aligned} \tag{19}$$

246 are the Euclidean norms of the parameters. The odd parameters correspond to the coupling terms inferred  
247 for  $\varphi_1$  in the direction  $2 \rightarrow 1$ , and the even parameters correspond to the coupling terms inferred for  $\varphi_2$  in  
248 the direction  $1 \rightarrow 2$ . See [32] for further details and an in depth tutorial on dynamical Bayesian inference  
249 and its implementation.

250 In summary, Bayesian inference is applied to  $\varphi_x^*$  and  $\varphi_x^{A*}$ , following their extraction from the time  
251 series (see Section 3.3). The time-evolution of the coupling parameters for each phase is inferred and  
252 these are used to determine the synchronization state of the system, and the direction of coupling between  
253 the phases. In a chronotaxic system we require the driver and response systems to be almost or fully  
254 synchronized, and also that the direction of coupling is only from the driver  $\varphi_x^A$  to  $\varphi_x$ .

255 The basis of this method is the calculation of the synchronization and direction of coupling of the  
256 system in order to determine chronotaxicity. However, the more synchronized the driver is with the  
257 response system, the less information flow between the two. With less information from which to infer  
258 parameters, most directionality methods, including Bayesian inference, become less reliable, and whilst  
259 synchronization may still be accurately detected, the direction of coupling will become less accurate the  
260 closer the system gets to synchronization. With frequent external perturbations, intermittent transitions,  
261 and moderate dynamical noise, there is greater information flow, and thus the inference is more precise,  
262 but this cannot be assumed in chronotaxic systems. In real systems, the synchronization state is not  
263 known beforehand, thus a more robust method is required, which can identify chronotaxicity even in  
264 systems close to synchronization.

## 265 3.5. Phase fluctuation analysis

266 Phase fluctuation analysis is effective even when  $\varphi_x$  and  $\varphi_p$  are almost synchronized. Given the  
 267 estimates of  $\varphi_x$  and  $\varphi_x^A$ , the next step is to analyse  $\Delta\varphi_x = \varphi_x^* - \varphi_x^{A*}$  to find the distribution of fluctuations  
 268 in the system relative to the unperturbed trajectory.

269 In order to quantify the distribution of fluctuations, detrended fluctuation analysis (DFA) can be  
 270 performed on  $\Delta\varphi_x$  [6,33]. Following from the observations of Section 3.2, this method tries to estimate  
 271 the fractal self-similarity of fluctuations at different timescales in order to distinguish the random walk  
 272 fluctuations of non-chronotaxic systems from the less-integrated fluctuations of chronotaxic systems.  
 273 The scaling of these fluctuations is determined by the self-similarity parameter  $\alpha$ , where fluctuations at  
 274 timescales equal to  $t/a$  can be made similar to those at the larger timescale  $t$  by multiplying with the  
 275 factor  $a^\alpha$ .

In order to calculate  $\alpha$  the time series  $\Delta\varphi_x$  is integrated in time and divided into sections of length  
 $n$ . For each section the local trend is removed by subtracting a fitted polynomial – usually a first order  
 linear fit [6,33]. The root mean square *fluctuation* for the scale equal to  $n$  is then given by

$$F(n) = \sqrt{\frac{1}{N} \sum_{i=1}^N Y_n(t_i)^2}, \quad (20)$$

276 where  $Y(t)$  is the integrated and detrended time series and  $N$  is its length. The fluctuation amplitude  
 277  $F(n)$  follow a scaling law if the time series is fractal. By plotting  $\log F(n)$  against  $\log n$ , the value of  $\alpha$   
 278 is simply the gradient of the line. For completely uncorrelated white Gaussian noise (the noise assumed  
 279 to perturb the system) the parameter for  $\alpha$  has a value of 0.5, while integrated white Gaussian noise  
 280 (expected in non-chronotaxic systems) returns a value of 1.5. Note that this assumes the noise does not  
 281 cause phase slips in  $\varphi_x$ . This would cause perturbations over large timescales (i.e. greater than one  
 282 cycle) to not decay even if the system was chronotaxic. In these cases another approach should be used  
 283 instead [14].

284 If there are large perturbations which cause the system to move far enough forward or behind the  
 285 current cycle to be attracted instead by an adjacent cycle, known as a phase slip, this will result in  
 286 an increased DFA exponent. This can result from large jumps in the extracted phase fluctuations. To  
 287 distinguish between this case, a chronotaxic system with phase slips, and a non-chronotaxic system, we  
 288 consider the fact that in the latter, perturbations may cause  $\Delta\varphi_x$  to change by  $2\pi$ , but these are part of  
 289 a continuous probability distribution, in contrast to the chronotaxic case. Phase slips can be detected by  
 290 calculating the distribution of the difference between the phase fluctuations  $\Delta\varphi_x(t)$  and these fluctuations  
 291 delayed by a timescale  $\tau$ .  $d\Delta\varphi_x^\tau(t) = \Delta\varphi_x(t + \tau) - \Delta\varphi_x(t)$  therefore gives information about the  
 292 perturbations of the system over that timescale. When phase slips are present, the distribution of  $|d\Delta\varphi_x^\tau|$   
 293 changes with respect to  $\tau$  [14]. An example of this difference is shown in Fig. 2 (g) & (h), and can also  
 294 be seen in real biological systems, as previously demonstrated in the heart rate variability [14].

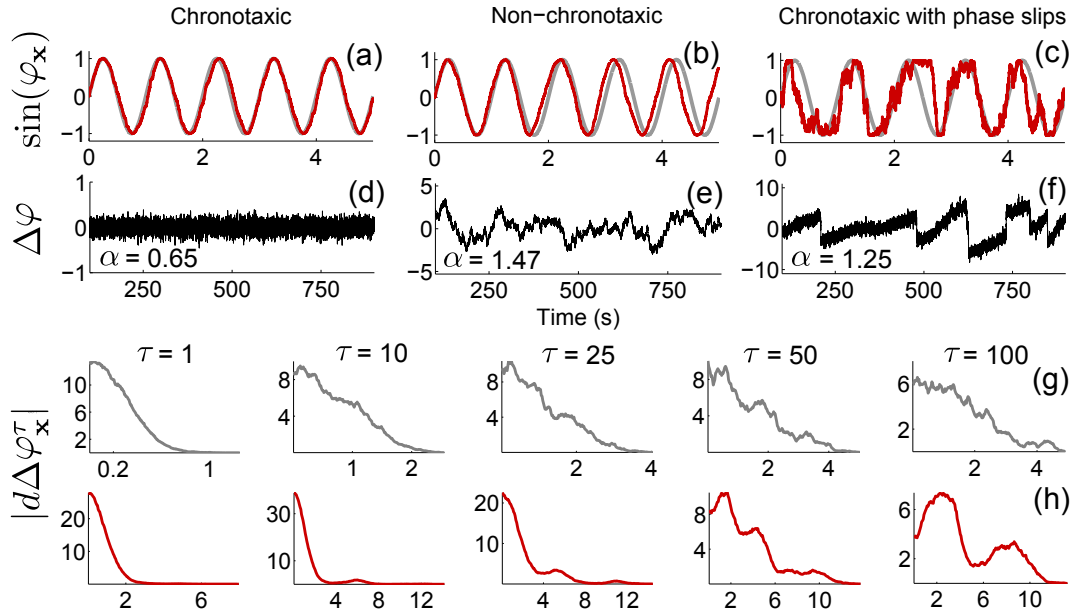


**Figure 2.** (a)–(c) 5 second time series of  $\sin(\varphi_x)$  (red line) in 3 cases: chronotaxic, non-chronotaxic, and chronotaxic with phase slips, from Eq. 21. The grey line shows  $\varphi_p$  (chronotaxic), and  $\omega_x t$  (non-chronotaxic). (d)–(f)  $\Delta\varphi_x$  for the whole time series, detrended with a moving average of 200s. In all cases  $\omega_{x,p} = 2\pi$ ,  $h = 0.001$ ,  $L = 1000$  seconds and  $\sigma = 0.3$ .  $\varepsilon = 5$  and  $0$  in the chronotaxic and non-chronotaxic cases, respectively. DFA exponents,  $\alpha$ , are shown. The DFA exponent of (f) incorrectly suggests the system is non-chronotaxic. To distinguish between a non-chronotaxic system and a chronotaxic system with phase slips, the delayed distributions were calculated (see Section 3.5) in the non-chronotaxic (g) and chronotaxic (h) case.

## 295 4. Application of inverse approach methods

### 296 4.1. Numerical simulations

297 The basis of the phase fluctuation analysis (PFA) method is the quantification of the fundamental  
 298 difference between phase fluctuation distributions in oscillatory systems, depending on their  
 299 chronotaxicity. Here, we illustrate this characteristic using the simplest realisation of a chronotaxic  
 300 system, two unidirectionally coupled oscillators (see Fig. 1(b)):

$$\begin{aligned}\dot{\varphi}_p &= \omega_p \\ \dot{\varphi}_x &= \omega_x - \varepsilon \sin(\varphi_x - \varphi_p) + \eta(t),\end{aligned}\quad (21)$$

301 where  $\varphi_p$  and  $\varphi_x$  are the instantaneous phases of the driving and the driven oscillators, respectively,  
 302  $\omega_p > 0$  and  $\omega_x > 0$  are the natural frequencies of the oscillators,  $\varepsilon > 0$  is the strength of the coupling and  
 303  $\eta$  is white Gaussian noise with standard deviation  $\sigma = \sqrt{2E}$  where  $\langle \eta(t) \rangle = 0$ ,  $\langle \eta(t)\eta(\tau) \rangle = \delta(t - \tau)E$ .  
 304 Note that when  $\varepsilon = 0$  the system is reduced to  $\dot{\varphi}_x = \omega_x + \eta(t)$  and becomes non-chronotaxic; when  
 305  $\eta = 0$  and  $\varepsilon > |\omega_x - \omega_p|$  the system becomes chronotaxic with  $\varphi_x^A(t) = \varphi_p(t) + \arcsin((\omega_p - \omega_x)/\varepsilon)$ .  
 306 The system was integrated using the Heun scheme [15], with an integration step of 0.001 and noise

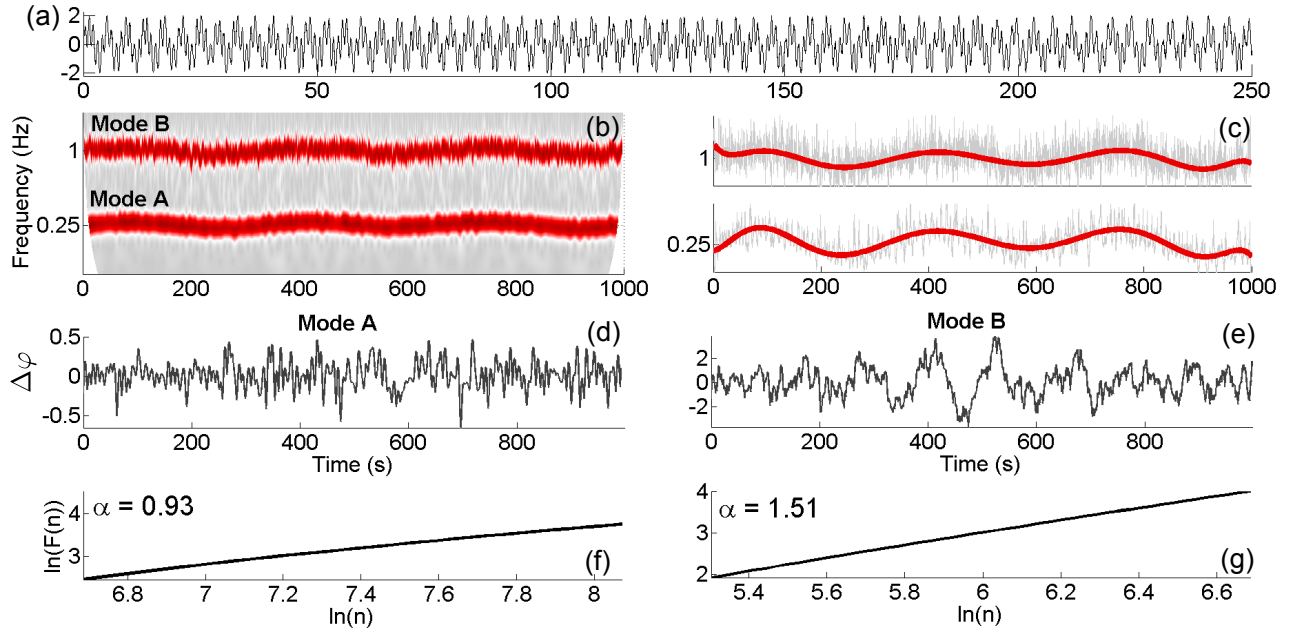


**Figure 3.** Identifying chronotaxicity in signals with more than one oscillatory mode. (a) First 250 seconds of a time series of a simulated signal containing two distinct oscillations, with coupling strengths  $\varepsilon = 2$  for mode A (chronotaxic) and  $\varepsilon = 0$  for mode B (non-chronotaxic). (b) The continuous wavelet transform of the signal in (a). (c) The instantaneous frequency (light grey) of both components is extracted from the wavelet transform, with central frequency  $f_0 = 0.5$ , and smoothed (red), using a polynomial fit. The smoothed frequency is then integrated in time to obtain an estimate of the unperturbed phase,  $\varphi_x^{A*}$ , which is then subtracted from the perturbed phase  $\varphi_x^*$  as extracted directly from the wavelet transform. (d) & (e) show  $\Delta\varphi_x = \varphi_x^* - \varphi_x^{A*}$  for each mode. (f) & (g) show the results of DFA analysis on  $\Delta\varphi_x$ , with DFA exponents  $\alpha$  correctly identifying mode A as chronotaxic and mode B as not chronotaxic.

307 strength  $\sigma = 0.3$ .  $\Delta\varphi_x$ , shown in Fig. 2, was obtained by subtracting the unperturbed phase ( $\varphi_x^A(t)$   
 308 and  $\omega_x t$  in the chronotaxic and non-chronotaxic cases, respectively) from the perturbed phase  $\varphi_x$ , as  
 309 obtained numerically. DFA analysis was then performed on  $\Delta\varphi_x$ , with exponents shown in Fig. 2.  
 310 The values of the exponents demonstrate the differences in the noise distributions between chronotaxic  
 311 and non-chronotaxic systems. In the chronotaxic case, the noise is closer to white, whereas in the  
 312 non-chronotaxic case it is closer to a random walk. It is this difference which is exploited in the PFA  
 313 method.

314 In many systems, particularly those originating from nature, there will be more than one oscillation  
 315 present in a signal, with different chronotaxicity characteristics. To test the PFA method in the case of  
 316 multiple modes a signal containing two distinct oscillations was simulated, with dynamics described by  
 317 Eq. 21, with time varying angular frequencies,

$$\begin{aligned}\dot{\omega}_{var}(t) &= A \cos(2\pi f_m t) + \eta(t) \\ \omega_{x,p}(t) &= 2\pi f_{p,x} + \omega_{var},\end{aligned}\tag{22}$$

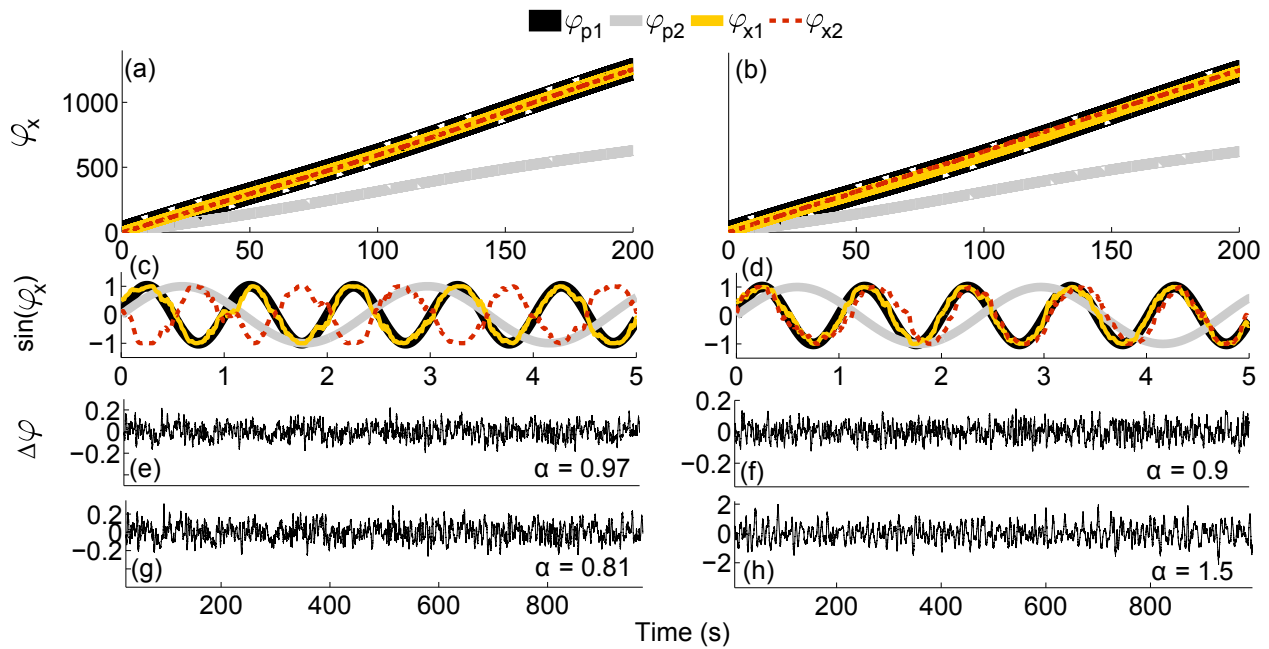


**Figure 4.** Identifying chronotaxicity using phase fluctuation analysis in a system of bidirectionally coupled oscillators. The system presented in Eq. 23 was simulated in two different states of chronotaxicity. (a) phase trajectories for the system when  $\varepsilon_1 = 0.1$ ,  $\varepsilon_2 = 20$ ,  $\varepsilon_3 = 0.1$  and  $\varepsilon_4 = 10$ . (b) phase trajectories of the system with  $\varepsilon_1 = 0.5$ ,  $\varepsilon_2 = 0.1$ ,  $\varepsilon_3 = 0.1$  and  $\varepsilon_4 = 15$ . (c) 5 seconds of the time series of both drivers and oscillators for parameters shown in (a). (d) 5 seconds time series for parameters shown in (b). (e) & (g) phase fluctuations from PFA on  $\sin(\varphi_{x1})$  and  $\sin(\varphi_{x2})$ , respectively. (f) & (h) phase fluctuations extracted with PFA on  $\sin(\varphi_{x1})$  and  $\sin(\varphi_{x2})$ , respectively.

318 where  $f_p$  and  $f_x$  are the average frequencies of oscillation in Hz of the chronotaxic and non-chronotaxic  
 319 case, respectively, and  $f_m$  is the frequency of variation. Frequencies of oscillation were chosen to vary  
 320 around 1 and 0.25 Hz in the non-chronotaxic and chronotaxic cases, respectively, with  $f_m = 0.003$ . Both  
 321 systems were perturbed with white Gaussian noise with strength  $\sigma = 0.5$ . The logarithmic frequency scale  
 322 of the wavelet transform is very useful for identifying and separating the presence of oscillatory modes,  
 323 which may otherwise appear as merged in other time-frequency representations, such as the windowed  
 324 Fourier transform. Fig. 3 shows the results of PFA analysis on the signal. It correctly identifies mode A  
 325 (around 0.25 Hz) as chronotaxic, and mode B (around 1 Hz) as non-chronotaxic.

326 In single variable time series obtained from real dynamical systems, it is highly unlikely that the  
 327 observed dynamics will result from a simple, unidirectional constant coupling as described above.  
 328 Rather, the system may be influenced by continuous perturbations, couplings to other oscillators, and  
 329 temporal fluctuations in chronotaxicity. Here, we demonstrate the applicability of the described inverse  
 330 approach methods to these more complex cases. We model a system of two bidirectionally coupled  
 331 oscillators

$$\begin{aligned}
\dot{\varphi}_{p1} &= \omega_{p1} \\
\dot{\varphi}_{p2} &= \omega_{p2} \\
\dot{\varphi}_{x1} &= \omega_{x1} + \varepsilon_1 \sin(\varphi_{x1} - \varphi_{x2}) - \varepsilon_4 \sin(\varphi_{x1} - \varphi_{p1}) + \eta(t) \\
\dot{\varphi}_{x2} &= \omega_{x2} + \varepsilon_2 \sin(\varphi_{x2} - \varphi_{x1}) - \varepsilon_3 \sin(\varphi_{x2} - \varphi_{p2}) + \eta(t),
\end{aligned} \tag{23}$$

332 with drivers  $\varphi_{p1}$  and  $\varphi_{p2}$ , and  $\omega_{p1}(t) = 2\pi - 0.5 \sin(2\pi 0.005(t))$  and  $\omega_{p2}(t) = \pi - 0.5 \cos(2\pi 0.005(t))$ .  
333 First, we consider the case of strong influence of the driver  $\varphi_{p1}$  on the system, resulting in chronotaxicity  
334 of both oscillators. Phase fluctuation analysis was applied to the system, and successfully identified both  
335  $\varphi_{x1}$  and  $\varphi_{x2}$  as chronotaxic (see Fig. 4(a)).

336 Second, we consider the case in which  $\varphi_{x1}$  is chronotaxic but  $\varphi_{x2}$  is not, and demonstrate that  
337 despite continuous influences from multiple drivers and other oscillators, single variable time series  
338 arising from the same system can be distinguished in terms of their chronotaxic dynamics. Again, PFA  
339 correctly distinguishes between the two oscillators. This could be of great importance when investigating  
340 composite parts of a larger dynamical system, and seeking to identify causal relationships between  
341 observed oscillations. For example, recent advances in cellular imaging are providing the means to  
342 observe the dynamics of individual cellular processes in different cellular compartments [34]. Applying  
343 inverse approach methods for the detection of chronotaxicity to these dynamics could provide valuable  
344 information on the current state of the cell.

345 So far, we have only considered scenarios in which a system constantly remains as either chronotaxic  
346 or non-chronotaxic. Real dynamical systems may exhibit time variation in their coupling strengths,  
347 allowing the system to fluctuate between chronotaxic states. In these cases, it is possible to use dynamical  
348 Bayesian inference to track variations in chronotaxicity in time. To demonstrate this,  $\varepsilon_3$  was allowed to  
349 vary in time in Eq. 23, whilst  $\varepsilon_1 = \varepsilon_2 = 0.1$  and  $\varepsilon_4 = 0$ , resulting in intermittent chronotaxicity of the  
350 oscillator  $\varphi_{x2}$ .  $\varphi_{x2}^{A*}$  and  $\varphi_{x2}^*$  were extracted from the synchrosqueezed wavelet transform of  $\sin(\varphi_{x2})$ .  
351 Results of the application of dynamical Bayesian inference are shown in Fig. 5. This method is able  
352 to track the intermittent changes in chronotaxicity, through changes in synchronization and direction  
353 of coupling, demonstrating its usefulness for the detection of chronotaxicity in systems where the  
354 interactions between oscillators are time-varying.

#### 355 4.2. Practical considerations

356 Both presented methods, phase fluctuation analysis and dynamical Bayesian inference, rely on precise  
357 phase extraction of the estimated attractor  $\varphi_x^{A*}$  and the perturbed dynamics  $\varphi_x^*$ . Therefore, the parameters  
358 in the respective methods must be carefully selected depending on the characteristics of the given data.

359 The continuous wavelet transform provides an optimal compromise between time and frequency  
360 resolution. In the majority of examples used in this paper,  $f_0 = 1$  has been used. However, the wavelet  
361 central frequency,  $f_0$ , can be altered to suit specific needs. For example, in a case where there are  
362 many phase slips, it may be necessary to extract the estimate of the attractor,  $\varphi_x^{A*}$ , with a higher  $f_0$  to  
363 obtain a better frequency resolution and smoother dynamics, whilst the perturbed phase  $\varphi_x^*$  is extracted  
364 using a lower  $f_0$ , leading to an increased time resolution for the purpose of locating each phase slip. The

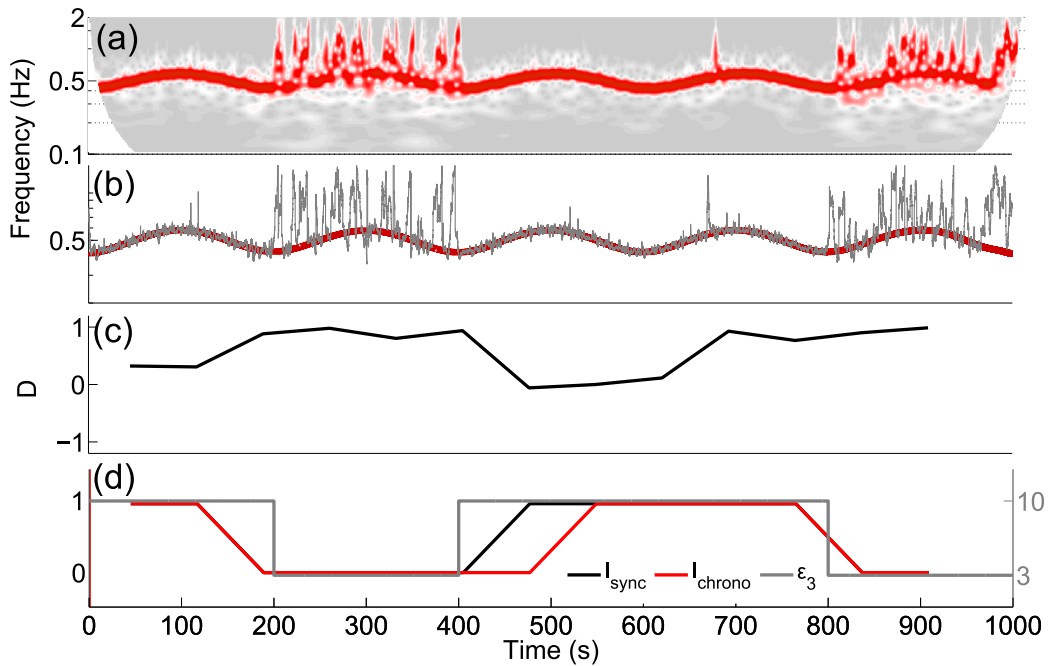


**Figure 5.** Identifying intermittent chronotaxicity using dynamical Bayesian inference. Bayesian inference was performed on  $\varphi_{x2}^*$  and  $\varphi_{x2}^{A*}$  extracted from  $\sin(\varphi_{x2})$  (Eqs. 23) with  $\varepsilon_3$  varying as shown in (d). (a) the CWT of  $\sin(\varphi_{x2})$ . (b) Instantaneous frequencies extracted from the wavelet transform.  $\varphi_{x2}^{A*}$  was extracted with  $f_0 = 2$  and smoothed using a polynomial fit (red line), whilst  $\varphi_{x2}^*$  was extracted from the wavelet transform with  $f_0 = 0.5$  (grey line). Bayesian inference was applied, using a time window of 90 seconds. The inferred direction of coupling can be seen in (c). Positive values show coupling from the driver to the oscillator only. (d)  $I_{\text{sync}}$  was calculated and shows excellent agreement with changes in  $\varepsilon_3$ .  $I_{\text{chrono}}$  was also calculated, and was slightly less accurate due to the direction of coupling becoming negative very briefly, due to reduced information flow between systems to accurately infer parameters during synchronization.

365 parameter  $f_0$  may also be increased to provide greater distinction between oscillatory modes, but this will  
 366 be at the expense of time resolution. It should be noted that modes must be separable in time-frequency  
 367 representations in order for these inverse approach methods to be applicable.

368 One fundamental assumption of chronotaxicity is that the system under consideration is oscillatory.  
 369 Although the presented methods can be applied to any extracted phases, one should take great care to  
 370 ensure that these phases correspond to a true oscillatory mode, otherwise all results will be meaningless.  
 371 In the numerical simulations presented here, we predetermine the characteristics of the oscillations which  
 372 are present, and ensure that they are not concealed by noise, allowing their successful extraction directly  
 373 from the wavelet transform. These extracted phases can be verified using the specified parameters as a  
 374 reference signal, and thus we can be confident with the final results. On the contrary, in real experimental  
 375 data, the first question must be whether the signal contains any significant oscillations at all. To determine  
 376 whether this is the case, the recently developed method of nonlinear mode decomposition (NMD) may be  
 377 used. NMD is an adaptive, time-frequency representation based decomposition tool, which decomposes  
 378 any given signal into a set of physically meaningful oscillations (if present) and residual noise. In the  
 379 detection of chronotaxicity, the crucial advantage of NMD over other decomposition methods, such as

empirical mode decomposition (EMD) or bandpass filtering, is its use of surrogate data testing in order to distinguish between deterministic and random activity [35]. The success of surrogate testing for the identification of nonlinear oscillatory modes in neural data has also been demonstrated previously [36], and more generally in [37]. By verifying the presence of oscillations, and their underlying nature, e.g. whether they are nonlinear, these methods reliably inform the user which analysis approach to take. In this way, we can ensure that any oscillatory modes extracted from real experimental data are physically meaningful, and their characteristics, including their instantaneous phase, are accurately determined. Once a significant oscillatory mode has been located and extracted using NMD, its smoothed instantaneous frequency provides  $\varphi_x^{A*}$  for use in phase fluctuation analysis.  $\varphi_x^*$  can then be extracted from the wavelet transform as before, with the parameter  $f_0$  chosen to give sufficient time resolution to follow the noise fluctuations which are removed by NMD. An example of the use of NMD in PFA is provided in Fig. 7, and explained further in Section 4.3.

The reliability of the presented inverse approach methods increases with data availability, i.e. a longer time series will give a more reliable result. However, when recording data from biological systems, it is not often feasible to collect hundreds of cycles of oscillation. When recording data from live subjects, for example blood flow recordings, the time of recording must be a compromise between long time series and subject comfort. In the case of cellular recordings, such as cell membrane recordings via the patch clamp technique, the health of the cell can rapidly deteriorate, and thus affect the reliability of results. Therefore, it is useful to determine the lowest possible number of recorded oscillations for which we may still reliably test for chronotacticity.

In order to address this question, two unidirectionally coupled phase oscillators (Eq. 21) were simulated for 1000 cycles with frequencies 1 and 0.1 Hz, with  $h = 0.01$  and  $\sigma = 0.07$ . With coupling  $\varepsilon = 2$ , the system is chronotactic. The important parameters to consider in DFA are  $n_{\min}$  and  $n_{\max}$ , the lower and upper values for the range of the first order polynomial fits performed in order to calculate  $\Delta\varphi_x$ . The lower value,  $n_{\min}$ , is set to be 2 cycles of the slowest oscillation, to ensure observation of the dynamics over a longer range than one cycle. The smallest  $n_{\max}$  required to still obtain a reliable DFA exponent was observed to be  $n_{\max} = 3$  cycles of oscillation (see Fig. 6), provided that the time series is sufficiently long. The second test seeks to identify the required length of the whole time series when using these values of  $n_{\min}$  and  $n_{\max}$  in DFA. The DFA exponent was calculated from varying lengths of the same noise signals, from 3 to 10 times  $n_{\max}$ , to identify the point where the result is no longer reliable. It was found that the time series should be at least 8 times  $n_{\max}$  in order to obtain a reliable result, therefore at least 24 cycles of the slowest oscillation are required to test for chronotacticity. However, if possible, the time series should be at least 10 times  $n_{\max}$  [38], to reduce noise by providing more data windows. Overlapping within DFA is also possible, and will go some way toward reducing noise, and improve reliability. The results shown in Fig. 6 were obtained with an overlap of 0.8.

Whilst we expect the value of the DFA exponent  $\alpha$  to be around 0.5 in a chronotactic system, and 1.5 in a non-chronotactic system, it is unlikely to be so definitive in reality. In fact, the value of  $\alpha$  will depend on a number of factors. The type of noise in a real system is not necessarily white, however the point of phase fluctuation analysis is to identify changes in its distribution.  $\alpha$  will also vary depending on how strong the chronotacticity is in the system, i.e., how strongly driven the observed oscillator is. In our models, this can be represented by varying the coupling strength  $\varepsilon$ ; weaker coupling will result

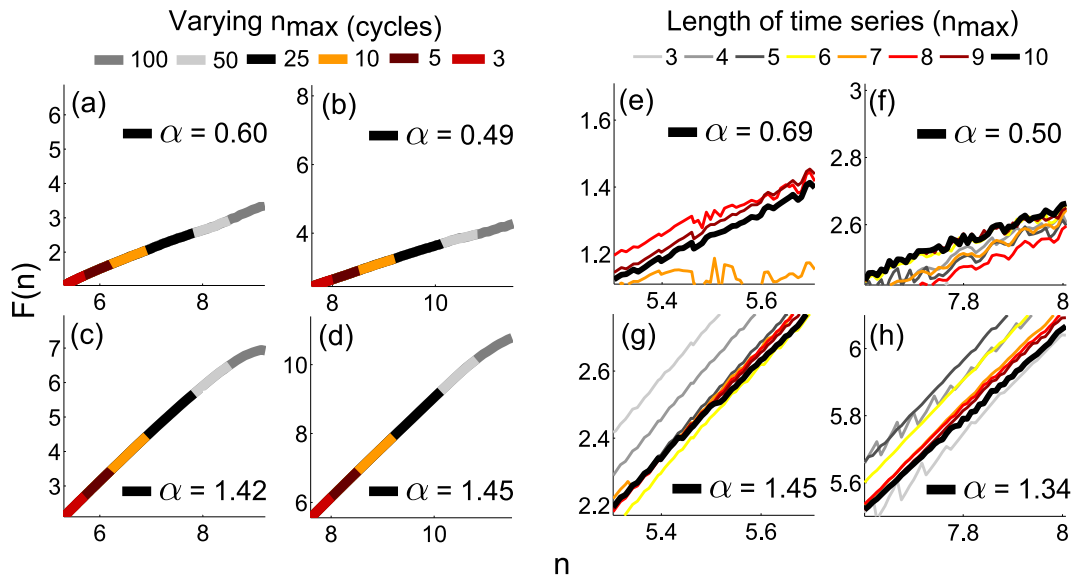


**Figure 6.** In order to test the reliability of the DFA exponent when reducing  $n_{\max}$ , the maximum number of cycles of oscillation used in its calculation was varied. (a) chronotaxic oscillation of 1 Hz. (b) chronotaxic oscillation of 0.1 Hz. (c) non-chronotaxic oscillation of 1 Hz. (d) non-chronotaxic oscillation of 0.1 Hz. The same noise signals were then tested with  $n_{\max} = 3$  for different lengths of the time series from 10 to 3 times  $n_{\max}$ . Based on these results, the time series should be at least 8 times  $n_{\max}$ , thus, there should be at least 24 oscillations in the time series. However, to ensure universal applicability, the length of the time series should be at least 10 times  $n_{\max}$ , the generally accepted value in DFA [38], resulting in the requirement of 30 cycles.

421 in a higher DFA exponent as the noise is partially integrated. The ratio of the natural frequency of the  
 422 chronotaxic oscillator to the frequency of the external driver, or detuning, may also affect the value of  $\alpha$ .

#### 423 4.3. Application to experimental data

424 Chronotaxicity will manifest in nature as a result of a driving system which is strong enough such that  
 425 the oscillatory response system maintains stability in its frequency and amplitude, even when subject  
 426 to continuous external perturbations. Chronotaxicity was previously demonstrated in the heart rate  
 427 variability (HRV) [14], when influenced by paced breathing. It has been shown that the main direction  
 428 of coupling between the cardiac and respiratory oscillators is the influence of the respiration on the heart  
 429 rate, known as respiratory sinus arrhythmia (RSA), and this was clearly demonstrated. Here, we provide  
 430 an example of the application of phase fluctuation analysis to real experimental data, in the form of an  
 431 electroencephalogram (EEG) recording from an anaesthetised human subject.

432 Distinct oscillations have long been observed in the brain since the invention of EEG by Hans Berger  
 433 in 1924. Briefly, from lowest to highest frequency, there are at least 5 frequency bands which have been  
 434 identified in approximately the following frequency intervals: delta (0.8–4 Hz), theta (4–7.5 Hz), alpha  
 435 (7.5–14 Hz), beta (14–22 Hz) and gamma (22–80 Hz). Different frequencies of oscillation have been  
 436 attributed to distinct states of the brain. For example, the alpha and theta bands have been shown to reflect  
 437 cognitive and memory performance [39]. One active area of research utilising the information provided

438 by these oscillations is in attempts to quantify the depth of anaesthesia based on their temporal evolution  
439 in different states of consciousness. Despite the worldwide use of general anaesthesia (GA) daily, the  
440 mechanisms leading to this state are still poorly understood in terms of how it truly affects the brain.  
441 Thus, brain-state monitoring is still not an accepted practice in GA, due to the lack of reliable markers  
442 [40]. However, recent studies in which the spectral power of the oscillations in different frequency bands  
443 has been tracked both temporally and spatially during anaesthesia with propofol have shown promising  
444 results. For example it was shown that during consciousness, alpha oscillations are concentrated in  
445 occipital channels, whilst during propofol induced anaesthesia, these oscillations are concentrated in  
446 frontal channels [40]. An increase in power in the frequency interval 0.1–1 Hz (delta) was also observed  
447 in this study during anaesthesia. Understanding the mechanisms underlying these changes in brain  
448 function could not only lead to new approaches to anaesthesia monitoring but may be widely applicable  
449 in many areas of neuroscience, including in the study of various neurological disorders.

450 It has been clearly demonstrated that phase interactions are highly important for healthy brain  
451 functioning, with by far the most widely reported observations revolving around phase synchronization,  
452 which can, as an example, be used to infer information about short and long range behaviours [41].  
453 Brain waves arise from networks of synchronized neurons, and the detected phase of these oscillations  
454 determines the degree of excitability of the neurons, and influences precise discharge times of the cells  
455 in the network, therefore affecting relative timing of action potential in different brain regions [42].

456 Before any conclusions may be drawn about the phase dynamics of a system, the phase must be  
457 accurately extracted from the time series. The problem of the extraction of phase from EEG data has  
458 been approached from many directions, some more physically meaningful than others. Early approaches  
459 to the investigation of phase interactions between brain waves used spectral coherence, but this does  
460 not separate phase and amplitude components, thus amplitude effects may influence coherence values  
461 when only phase locking information is required [43]. A widely used phase extraction approach is the  
462 use of the Hilbert transform to obtain the analytic signal [44], usually preceded by band-pass filtering  
463 in the frequency interval of interest, highlighting the necessity of the separation of the oscillation of  
464 interest from background brain activity, either other oscillations or noise. Lachaux *et al.* recognised  
465 the necessity of the separation of amplitude and phase when seeking to detect synchrony between  
466 brain waves, introducing phase-locking statistics (PLS) [43] to measure the phase covariance between  
467 two signals, verified by surrogate testing. This method also allows for non-stationarity in the signal.  
468 However, based on very narrow band-pass filtering, this method does not allow for time-variability in  
469 the frequency of oscillation, but did highlight the usefulness of complex wavelets in the extraction of  
470 phase dynamics. The Hilbert transform and wavelet convolution methods were compared in the analysis  
471 of neural synchrony, and found not to differ substantially [45], but both these methods relied on narrow  
472 band-pass filtering beforehand. However, the use of band-pass filtering to extract an oscillatory EEG  
473 component with a time-varying frequency has limited usefulness. An instantaneous frequency defined  
474 from the analytic signal obtained from band-passing in a particular frequency range in a real signal  
475 containing multiple spectral components and noise may be ambiguous and meaningless [41]. To address  
476 this problem, ridge extraction methods [29] applied to the complex wavelet transform were used to  
477 track the instantaneous frequency of a single oscillatory mode [41], providing a much higher precision  
478 of phase extraction, and importantly allowing the phase dynamics of nonautonomous systems to be

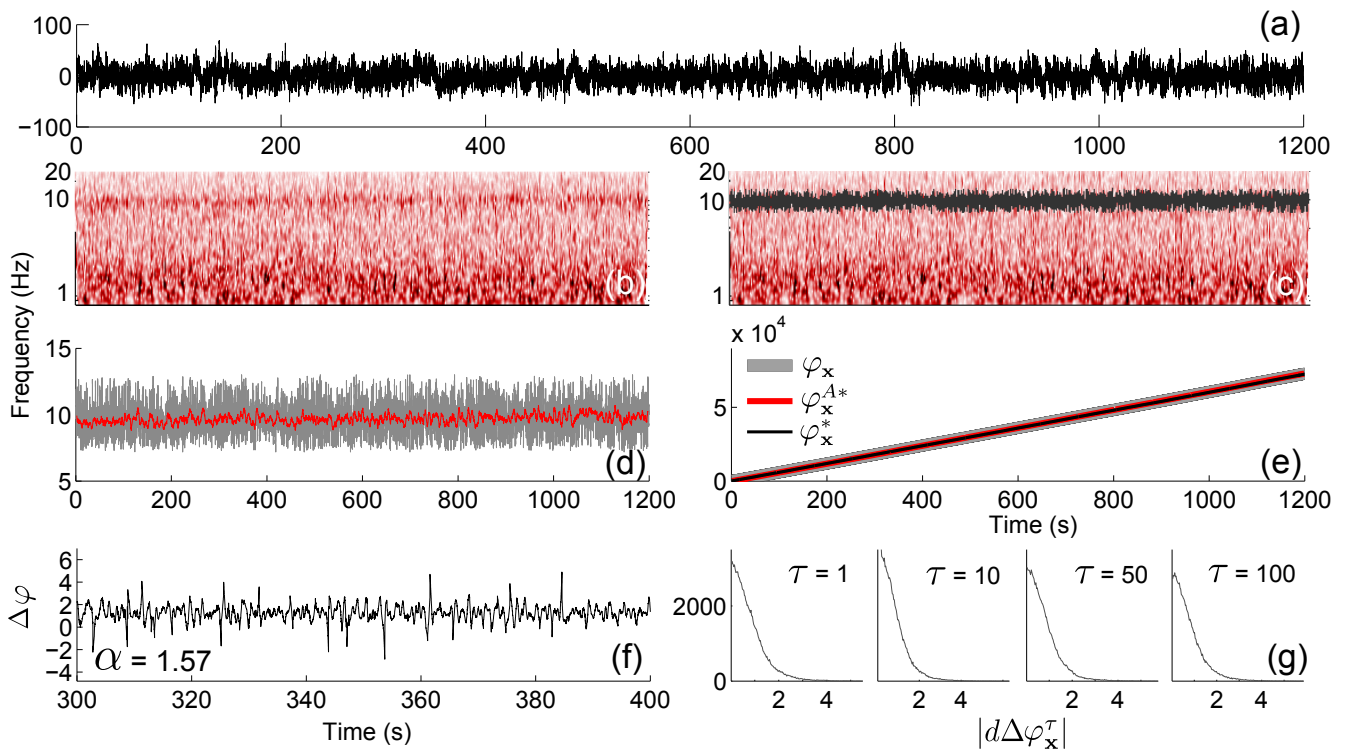


**Figure 7.** Example of the application of phase fluctuation analysis to an EEG signal obtained from the forehead of an anaesthetised patient, shown in (a). (b) The continuous wavelet transform of the EEG signal in (a). (c) Using nonlinear mode decomposition (NMD)(see text), a significant oscillatory mode in the alpha frequency band was identified and extracted (dark grey line). (d) The instantaneous frequency extracted using NMD (grey line), and smoothed using a moving average of 4 seconds (red line). (e) The extracted phases of the mode from NMD (grey), smoothed NMD (red), and from the CWT (black) with  $f_0 = 1.5$ . (f)  $\Delta\varphi_x$  was calculated as  $\varphi_x^* - \varphi_x^{A*}$ . The DFA exponent was calculated and was 1.57, suggesting that the system is not chronotaxic. Checking for phase slips in (g) shows no change in distribution.

479 accurately traced in time. Another, rarely considered, issue when tracing instantaneous frequencies in  
 480 time is the presence of high harmonics in the signal. Narrow restriction of the frequency range will  
 481 remove these harmonics, and thus remove valuable intra-cycle phase information. This issue has been  
 482 addressed directly by the introduction of nonlinear mode decomposition [35]. The inverse approach  
 483 methods applied here take into account all these issues in order to accurately extract the instantaneous  
 484 phase of brain oscillations.

485 In order to demonstrate the method and search for evidence of chronotaxicity in the phase dynamics  
 486 of brain waves we applied phase fluctuation analysis to a real EEG signal. The EEG of an anaesthetised  
 487 subject was recorded for 20 minutes at 1200 Hz (Fig.7(a)). The signal was resampled to 100 Hz by  
 488 splitting the time series into windows, and setting their mid-point to their mean. As expected, strong  
 489 oscillations were observed in the alpha and delta frequency bands. Nonlinear mode decomposition (see  
 490 Section 4.2) extracted the oscillatory mode around 10 Hz in the alpha frequency band and identified it  
 491 as physically meaningful through surrogate testing (Fig.7(c)). The instantaneous frequency of this mode  
 492 was then smoothed using a moving average of 4 seconds. This value was chosen to provide the best

493 match between the instantaneous phase of the extracted nonlinear mode  $\varphi_x$  and its smoothed version  
494  $\varphi_x^{A*}$ . As NMD by nature removes the noise from the modes which it extracts,  $\varphi_x^*$  must then be extracted  
495 from the continuous wavelet transform with a time resolution which will allow the noise fluctuations to be  
496 included in the extracted mode. Here, it is very important to check that the extracted phase corresponds  
497 to that extracted using NMD (see Fig. 7(e)). Once the viability of the extracted fluctuations is confirmed,  
498  $\Delta\varphi_x$  can be calculated as  $\varphi_x^* - \varphi_x^{A*}$ . The DFA exponent of  $\Delta\varphi_x$  was then calculated, and was 1.57. The  
499 distribution  $|d\Delta\varphi_x^T|$  was calculated to check for phase slips in the extracted phase fluctuations, but the  
500 distribution did not change over any timescale,  $\tau$ .

501 The analysis suggests that the alpha oscillation as extracted is not chronotaxic. However, the current  
502 inverse approach methods are based on a single point attractor and single response system. As discussed  
503 by Sheppard *et al.* [46], the spectral peaks observed in the EEG, including those observed in the alpha  
504 band, result from frequency synchronization between thousands of neurons. In this sense, the observed  
505 phase is in fact only a statistical measure, highlighting the preferred phase of the underlying ensemble  
506 of neurons. A method to quantify this was provided by the mean-field variability index,  $\kappa$ , which  
507 changes depending on the interactions in the observed network of oscillators [46]. For a non-interacting  
508 network, with purely random phasors,  $\kappa$  will converge to 0.215, whereas in a state of complete phase  
509 synchronization,  $\kappa$  will tend to zero. Based on the current assumptions of the inverse approach methods,  
510 if the detection of chronotaxicity relied only on phase dynamics, we would expect the value of  $\kappa$  to  
511 tend to zero in a chronotaxic system. However, when applied to real EEG data,  $\kappa$  was actually greater  
512 than 0.215 in most cases, suggesting amplitude synchrony (possibly intermittent), intermittent phase  
513 coherence, or both. Therefore, it is apparent that in the case of brain dynamics, to truly characterise  
514 chronotaxicity, it must be reconsidered within a network of many oscillators, as known to be present in  
515 the brain. Here, the driving system may be a subnetwork of synchronized oscillators or the mean-field  
516 or mean-phase of ensembles of neurons, influencing other areas of the brain in complex ways, with both  
517 temporal and spatial dynamics to take into account.

518 The presented methods are restricted by the fact that they are currently only applicable to determining  
519 chronotaxicity in phase dynamics. Traditionally, in brain dynamics, it is the amplitude of the oscillations  
520 observed in the distinct frequency bands which receives the most attention, although phase dynamics  
521 is now gaining considerable recognition [47]. In addition to the dynamics within individual frequency  
522 bands, there are also interactions between frequency bands [48], known as cross frequency coupling  
523 (CFC). The importance of phase information in oscillatory brain activity has been clearly demonstrated,  
524 for example phase synchronization between frequencies has been shown to be correlated with certain  
525 cognitive processes [49]. Phase measures also provide the advantage of high temporal precision [49].  
526 However, the nature of CFCs have not only been observed as phase-phase interactions [50], but also as  
527 amplitude-phase [51] and amplitude-amplitude interactions [52]. Whilst some efforts have been made  
528 to isolate phase information in neural oscillations [53], the importance of amplitude-phase interactions  
529 cannot be ignored, for example the observed modulation of gamma amplitude by the phase of theta  
530 oscillations has been identified as a code utilised in multi-item formation in the brain [54]. Other  
531 functional roles of amplitude-phase coupling have also been highlighted [55], thus it is clear that both  
532 amplitude and phase must be considered simultaneously to accurately characterise brain dynamics.

533 Indeed, phase-amplitude coupling has been demonstrated during anaesthesia [56], meaning that the  
534 current inverse approach methods may be insufficient to determine chronotaxicity in this system.

## 535 **5. Discussion**

536 The recent formulation of chronotaxic systems provides a completely novel approach to the  
537 characterisation of time-varying dynamics in real data. Crucially, they provide a framework in which  
538 systems may be time-varying, both in terms of their amplitude and phase dynamics, continuously  
539 perturbed, and yet still exhibit determinism. Whilst the apparent complexity of some real time-varying  
540 oscillatory systems previously led to their consideration as stochastic or chaotic, chronotaxicity  
541 facilitates a much more natural approach to the description of their dynamics. The introduction of this  
542 approach required the development of new inverse approach methods for the detection of chronotaxicity  
543 in time series arising from dynamical systems. Here, we reviewed the currently available methods for the  
544 identification of chronotaxicity from a single time series, and also expanded on various issues regarding  
545 their implementation, in order to facilitate the application of the methods to any data set containing at  
546 least one oscillatory component. This ability to characterise oscillations in terms of their chronotaxicity,  
547 i.e. to determine whether the observed dynamics arise as a result of influence from an external driver,  
548 provides the potential to unlock new information about dynamical systems and their interactions with  
549 their environment.

550 As they currently stand, the inverse approach methods for the detection of chronotaxicity are only  
551 applicable in systems in which the amplitude and phase dynamics are separable, as they are applied  
552 directly to the extracted phases of the system, and all amplitude information is discarded. This  
553 assumption is valid if considering that the amplitude dynamics of a chronotaxic system corresponds  
554 to the convergence of the system to the limit cycle, influenced only by a negative Lyapunov exponent  
555 and external perturbations, whilst the phase dynamics corresponds to convergence to the time-dependent  
556 point attractor, which is also characterized by a negative Lyapunov exponent and external perturbations,  
557 but also the motion of the point attractor itself [14]. As it is this point attractor in phase dynamics  
558 which we are interested in, separation of amplitude and phase follows naturally. Using this approach,  
559 an example of chronotaxic dynamics was successfully demonstrated in a real system, in the case  
560 of heart rate variability [14]. However, in generalized chronotaxic systems [12], the amplitude  
561 and phase are not required to be separable, providing even greater applicability to real systems,  
562 allowing amplitude-amplitude and amplitude-phase interactions, in addition to the phase-phase dynamics  
563 considered in [10,11]. Therefore, the incorporation of the ability to identify these new possibilities for  
564 chronotaxicity is crucial in the further development of these inverse approach methods. This will then  
565 provide the means to detect chronotaxicity in systems where amplitude and phase are not separable,  
566 as previously discussed in the case of brain dynamics (see Section 4.3). The current definition of  
567 chronotaxicity is based on a time-varying point attractor, exerting influence over a system such that it can  
568 remain stable despite continuous external perturbations. Numerical results presented here assume that  
569 this point attractor results from a single oscillatory drive system, acting on a maximum of two coupled  
570 oscillators. However, as highlighted in the brain dynamics example, in reality we must consider that this

571 point attractor could result from multiple interacting influences, for example a network of oscillators,  
572 perhaps acting as one synchronized drive system.

573     Regardless of the mechanisms of the underlying oscillations, if they manifest as a point attractor,  
574 characterisation of their chronotaxicity necessitates the application of methods which can extract both  
575 their phase and amplitude dynamics with utmost accuracy. Methods reliant on averaging will not provide  
576 the required precision. Both amplitude and phase information can be extracted from the continuous  
577 wavelet transform, a fact which may be utilised in the further development of inverse approach methods  
578 for the detection of chronotaxicity. Extending these methods to simultaneously take into account both  
579 phase and amplitude dynamics, whilst incorporating the effects of their couplings, may lead to a method  
580 based on an optimal combination of time-frequency representations and effective connectivity methods  
581 such as dynamical Bayesian inference. This will then provide even wider applicability to real oscillatory  
582 systems such as those observed in brain dynamics.

### 583 **Acknowledgments**

584     This work was supported by the Engineering and Physical Sciences Research Council (UK) (Grant  
585 No. EP/100999X1) and in part by the Slovenian Research Agency (Program No. P20232).

### 586 **Author Contributions**

587     Aneta Stefanovska conceived the research. Gemma Lancaster performed the analysis, prepared the  
588 figures, and with Philip Clemson and Yevhen Suprunenko wrote the manuscript. Tomislav Stankovski  
589 was involved in the implementation of dynamical Bayesian inference. All authors have read, commented  
590 on, and approved the final manuscript.

### 591 **Conflicts of Interest**

592     The authors declare no conflict of interest.

### 593 **References**

- 594 1. *Nonautonomous Dynamical Systems in the Life Sciences*. Kloeden, P. E., Pöetzsche, C., Eds.;  
595 Springer, 2013.
- 596 2. Friedrich, R.; Peinke, J.; Sahimi, M.; Tabar, M. R. R. Approaching complexity by stochastic  
597 methods: From biological systems to turbulence. *Phys. Rep.* **2011**, *506*, 87–162.
- 598 3. Wessel, N.; Riedl, M.; Kurths, J. Is the normal heart rate “chaotic” due to respiration? *Chaos* **2009**,  
599 *19*, 028508:1–028508:4.
- 600 4. Friston, K. A free energy principle for biological systems. *Entropy* **2012**, *14*, 2100–2121.
- 601 5. Kurz, F. T.; Aon, M. A.; O’Rourke, B.; Armoundas, A. A. Wavelet analysis reveals heterogeneous  
602 time-dependent oscillations of individual mitochondria. *Am. J. Physiol. - Heart and Circ. Physiol.*  
603 **2010**, *299*, H1736–H1740.
- 604 6. Shioyai, Y.; Stefanovska, A.; McClintock, P. V. E. Nonlinear dynamics of cardiovascular ageing.  
605 *Phys. Rep.* **2010**, *488*, 51–110.

- 606 7. Iatsenko, D.; Bernjak, A.; Stankovski, T.; Shiogai, Y.; Owen-Lynch, P. J.; Clarkson, P. B. M.;  
607 McClintock, P. V. E.; Stefanovska, A. Evolution of cardiorespiratory interactions with age. *Phil.*  
608 *Trans. R. Soc. A* **2013**, *371*, 20110622:1–20110622:18.
- 609 8. Stam, C. J. Nonlinear dynamical analysis of EEG and MEG: Review of an emerging field. *Clin.*  
610 *Neurophysiol.* **2005**, *116*, 2266–2301.
- 611 9. Stefanovska, A.; Bračić, M.; Kvernmo, H. D. Wavelet analysis of oscillations in the peripheral  
612 blood circulation measured by laser Doppler technique. *IEEE Trans. Bio. Med. Eng.* **1999**, *46*,  
613 1230–1239.
- 614 10. Suprunenko, Y. F.; Clemson, P. T.; Stefanovska, A. Chronotaxic systems: A new class of  
615 self-sustained non-autonomous oscillators. *Phys. Rev. Lett.* **2013**, *111*, 024101:1–024101:5.
- 616 11. Suprunenko, Y. F.; Clemson, P. T.; Stefanovska, A. Chronotaxic systems with separable amplitude  
617 and phase dynamics. *Phys. Rev. E* **2014**, *89*, 012922:1–012922:9.
- 618 12. Suprunenko, Y. F.; Stefanovska, A. Generalized chronotaxic systems: Time-dependent oscillatory  
619 dynamics stable under continuous perturbation. *Phys. Rev. E* **2014** *90*, 032921:1–032921:10.
- 620 13. Bishnani, Z.; Mackay, R. S. Safety criteria for aperiodically forced systems. *Dynam. Sys.* **2003**,  
621 *18*, 107–129.
- 622 14. Clemson, P. T.; Suprunenko, Y. F.; Stankovski, T.; Stefanovska, A. Inverse approach to chronotaxic  
623 systems for single-variable time series. *Phys. Rev. E* **2014**, *89*, 032904:1–032904:12.
- 624 15. Clemson, P. T.; Stefanovska, A. Discerning non-autonomous dynamics. *Phys. Rep.* **2014**, *542*,  
625 297–368.
- 626 16. Gabor, D. Theory of communication. *J. IEEE* **1946**, *93*, 429–457.
- 627 17. Sheppard, L. W.; Vuksanović, V.; McClintock, P. V. E.; Stefanovska, A. Oscillatory dynamics of  
628 vasoconstriction and vasodilation identified by time-localized phase coherence. *Phys. Med. Biol.*  
629 **2011**, *56*, 3583–3601.
- 630 18. Daubechies, I.; Lu, J.; Wu, H.-T. Synchrosqueezed wavelet transforms: An empirical mode  
631 decomposition-like tool. *Appl. and Comput. Harmon. Anal.* **2011**, *30*, 243–261.
- 632 19. Iatsenko, D.; McClintock, P. V. E.; Stefanovska, A. Linear and synchrosqueezed time-frequency  
633 representations revisited: Overview, standards of use, resolution, reconstruction, concentration and  
634 algorithms. *Digit. Signal Process.* **2015**, *In Press*
- 635 20. Stankovski, T.; Duggento, A.; McClintock, P. V. E.; Stefanovska, A. Inference of time-evolving  
636 coupled dynamical systems in the presence of noise. *Phys. Rev. Lett.* **2012**, *109*,  
637 024101:1–024101:5.
- 638 21. Duggento, A.; Stankovski, T.; McClintock, P. V. E.; Stefanovska, A. Dynamical Bayesian inference  
639 of time-evolving interactions: From a pair of coupled oscillators to networks of oscillators. *Phys.*  
640 *Rev. E* **2012**, *86*, 061126:1–061126:15.
- 641 22. Jamšek, J.; Paluš, M.; Stefanovska, A. Detecting couplings between interacting oscillators with  
642 time-varying basic frequencies: Instantaneous wavelet bispectrum and information theoretic  
643 approach. *Phys. Rev. E* **2010**, *81*, 036207:1–036207:10.
- 644 23. Friston, K. Functional and effective connectivity: A review. *Brain Connect.* **2011**, *1*, 13–36.
- 645 24. Kuramoto, Y. *Chemical oscillations, waves, and turbulence.*; Springer-Verlag, 1984.

- 646 25. Oppenheim, A. V.; Schaffer, R. W.; Buck, J. R. *Discrete-Time Signal Processing*; Prentice-Hall:  
647 Upper Saddle River, 1999.
- 648 26. Kralemann, B.; Cimponeriu, L.; Rosenblum, M.; Pikovsky, A.; Mrowka, R. Phase dynamics of  
649 coupled oscillators reconstructed from data. *Phys. Rev. E* **2008**, *77*, 066205:1–066205:16.
- 650 27. Kaiser, G. *A Friendly Guide to Wavelets*; Birkhäuser: Boston, 1994.
- 651 28. Morlet, J. Sampling theory and wave propagation. In *Issues on Acoustic Signal/Image Processing*  
652 *and Recognition* vol. I, NATO ASI series; Chen, C. H. Ed.; Springer: Berlin, 1983.
- 653 29. Delprat, N.; Escudie, B.; Guillemain, P.; Kronland-Martinet, R.; Tchamitchian, P.; Torrèsani, B.  
654 Asymptotic wavelet and Gabor analysis: Extraction of instantaneous frequencies. *IEEE Trans. Inf.*  
655 *Theory* **1992**, *38*, 644–664.
- 656 30. Carmona, R. A.; Hwang, W. L.; Torrèsani, B. Characterization of signals by the ridges of their  
657 wavelet transforms. *IEEE Trans. Sig. Proc.* **1997**, *45*, 2586–2590.
- 658 31. Rosenblum, M. G.; Pikovsky, A. S. Detecting direction of coupling in interacting oscillators. *Phys.*  
659 *Rev. E.* **2001**, *64*, 045202:1–045202:4.
- 660 32. Stankovski, T; Duggento, A; McClintock, P. V. E.; Stefanovska, A. A tutorial on time-evolving  
661 dynamical Bayesian inference. *Eur. Phys. J. Special Topics* **2014**, *223*, 2685–2703.
- 662 33. Peng, C. K.; Buldyrev, S. V.; Havlin, S.; Simons, M.; Stanley, H. E.; Goldberger, A. L. Mosaic  
663 organisation of DNA Nucleotides. *Phys. Rev. E* **1994**, *49*, 1685–1689.
- 664 34. Kioka, H.; Kato, H.; Fujikawa, M.; Tsukamoto, O.; Suzuki, T.; Imamura, H.; Nakano, A.; Higo, S.;  
665 Yamazaki, S.; Matsuzaki, T.; *et al.* Evaluation of intramitochondrial ATP levels identifies GO/G1  
666 switch gene 2 as a positive regulator of oxidative phosphorylation. *Proc. Natl. Acad. Sci. USA*  
667 **2014**, *111*, 273–278.
- 668 35. Iatsenko, D.; McClintock, P. V. E.; Stefanovska, A. Nonlinear mode decomposition: A  
669 noise-robust, adaptive decomposition method. *Submitted* **2015**.
- 670 36. Vejmelka, M.; Paluš, M.; Šušmáková, K. Identification of nonlinear oscillatory activity embedded  
671 in broadband neural signals. *Int. J. Neural Syst.* **2010** *20*, 117–128.
- 672 37. Paluš, M.; Novotná, D. Enhanced Monte Carlo Singular System Analysis and detection of period  
673 7.8 years oscillatory modes in the monthly NAO index and temperature records. *Nonlinear Proc.*  
674 *Geoph.* **2004**, *11*, 721–729.
- 675 38. Hardstone, R.; Poil, S-S.; Schiavone, G.; Jansen, R.; Nikulin, V. V.; Mansvelder, H. D.;  
676 Linkenkaer-Hansen, K. Detrended fluctuation analysis: A scale-free view on neuronal oscillations.  
677 *Front. Physiol.* **2012**, *3*, 450:1–450:13.
- 678 39. Klimesch, W. EEG alpha and theta oscillations reflect cognitive and memory performance: a review  
679 and analysis. *Brain Res. Rev.* **1999**, *29*, 169–195.
- 680 40. Purdon, P. L.; Pierce, E. T.; Mukamel, E. A.; Prerau, M. J.; Walsh, J. L.; Wong, K. F. K.;  
681 Salazar-Gomez, A. F.; Harrell, P. G.; Sampson, A. L.; Cimenser, A.; *et al.* Electroencephalogram  
682 signatures of loss and recovery of consciousness from propofol. *Proc. Natl. Acad. Sci. USA* **2013**,  
683 *110*, E1142–E1151.
- 684 41. Rudrauf, D.; Douiri, A.; Kovach, C.; Lachaux, J-P.; Cosmelli, D.; Chavez, M.; Adam, C.;  
685 Renault, B.; Martinerie, J.; Le Van Quyen, M. Frequency flows and the time-frequency dynamics  
686 of multivariate phase synchronization in brain signals. *NeuroImage* **2006**, *31*, 209–227.

- 687 42. Fell, J.; Axmacher, N. The role of phase synchronization in memory processes. *Nat. Rev. Neurosci.*  
688 **2011**, *12*, 105–118.
- 689 43. Lachaux, J-P.; Rodriguez, E.; Martinerie, J.; Varela, F. J. Measuring phase synchrony in brain  
690 signals. *Hum. Brain Mapp.* **1999**, *8*, 194–208.
- 691 44. Tass, P.; Rosenblum, M. G.; Weule, J.; Kurths, J.; Pikovsky, A.; Volkman, J.; Schnitzler,  
692 A.; Freund, H.-J. Detection of  $n:m$  phase locking from noisy data: Application to  
693 magnetoencephalography. *Phys. Rev. Lett.* **1998**, *81*, 3191–3294.
- 694 45. Le Van Quyen, M.; Foucher, J.; Lachaux, J-P.; Rodriguez, E.; Lutz, A.; Martinerie, J.; Varela, F.  
695 J. Comparison of Hilbert transform and wavelet methods for the analysis of neural synchrony. *J.*  
696 *Neurosci. Meth.* **2001**, *111*, 83–98.
- 697 46. Sheppard, L. W.; Hale, A. C.; Petkoski, S; McClintock, P. V. E.; Stefanovska, A. Characterizing  
698 an ensemble of interacting oscillators: The mean-field variability index. *Phys. Rev. E* **2013**, *87*,  
699 012905:1–012905:11.
- 700 47. Palva, S.; Palva, J. M. New vistas for  $\alpha$ -frequency band oscillations. *Trends Neurosci.* **2007**, *30*,  
701 150–158.
- 702 48. Stankovski, T.; Ticcinelli, V.; McClintock P. V. E.; Stefanovska, A. Coupling functions in networks  
703 of oscillators. *New J. Phys.* **2015**, *17*, 035002:1–035002:12.
- 704 49. Sauseng, P.; Klimesch, W. What does phase information of oscillatory brain activity tell us about  
705 cognitive processes? *Neurosci. Biobehav. R.* **2008**, *32*, 1001–1013.
- 706 50. Darvas, F.; Miller, K. J.; Rao, R. P. N.; Ojemann, J. G. Nonlinear phase-phase cross-frequency  
707 coupling mediates communication between distant sites in human neocortex. *J. Neurosci.* **2009**,  
708 *29*, 426–435.
- 709 51. Tort, A. B. L.; Komorowski, R.; Eichenbaum, H.; Kopell, N. Measuring phase-amplitude coupling  
710 between neuronal oscillations of different frequencies. *J. Neurophysiol.* **2010**, *104*, 1195–1210.
- 711 52. Friston, K. J. Another neural code? *NeuroImage* **1997**, *5*, 213–220.
- 712 53. Hurtado, J. M.; Rubchinsky, L. L.; Sigvardt, K. A. Statistical method for detection of phase-locking  
713 episodes in neural oscillations. *J. Neurophysiol.* **2004**, *91*, 1883–1898.
- 714 54. Lisman, J. E.; Jensen, O. The theta-gamma neural code. *Neuron* **2013**, *77*, 1002–1016.
- 715 55. Canolty, R. T.; Knight, R. T. The functional role of cross-frequency coupling. *Trends Cogn. Sci.*  
716 **2010**, *14*, 506–515.
- 717 56. Mukamel, E. A.; Pirondini, E.; Babadi, B.; Foon Kevin Wong, K.; Pierce, E. T.; Harrell, P. G.;  
718 Walsh, J. L.; Salazar-Gomez, A. F.; Cash, S. S.; Eskandar, E. N.; *et al.* A transition in brain state  
719 during propofol-induced unconsciousness. *J. Neurosci.* **2014**, *34*, 839–845.